Shear Stress Estimated by Quantitative Coronary Angiography Predicts Plaques Prone to Progress and Cause Events

Christos V. Bourantas[abc*], Thomas Zanchin[ade*], Ryo Torii[e], Patrick W. Serruys[f], Alexios Karagiannis[g], Anantharaman Ramasamy[ac], Hannah Safi[b], Ahmet Umit Coskun[h], Gerhard Koning[i], Yoshinobu Onuma[j], Christian Zanchin[d], Rob Krams[k], Anthony Mathur[ac], Andreas Baumbach[ac], Gary Mintz[i], Stephan Windecker[d], Alexandra Lansky[bm], Akiko Maehara[i], Gregg W. Stone[m]

[a] Department of Cardiology, Barts Heart Centre, Barts Health NHS, London, United Kingdom

[b] Institute of Cardiovascular Sciences, University College London, London, United Kingdom

[c] Centre for Cardiovascular Medicine and Device Innovation, Queen Mary University London, London, United Kingdom

[d] Department of Cardiology, Bern University Hospital, Bern, Switzerland

[e] Department of Mechanical Engineering, University College London, London, United Kingdom

[f] Faculty of Medicine, National Heart & Lung Institute, Imperial College London, United Kingdom

[g] CTU Bern, Institute of Social and Preventive Medicine, Bern University, Bern, Switzerland

[h] Mechanical and Industrial Engineering, Northeastern University, Boston, Massachusetts

[I] Medis medical imaging systems bv, Leiden, the Netherlands

[j] Department of Interventional Cardiology, Thoraxcenter, Erasmus Medical Center, Rotterdam, the Netherlands

[k] Department of Molecular Bioengineering Engineering and Material Sciences, Queen Mary University London, London, United Kingdom

[i] Department of Cardiology, Columbia University Medical Center and the Cardiovascular Research Foundation, New York, New York

[m] Division of Cardiovascular Medicine, Department of Internal Medicine, Yale School of Medicine, New Haven, Connecticut

[n] Cardiovascular Division, Brigham & Women's Hospital, Harvard Medical School, Boston, Massachusetts

Corresponding author

Christos V. Bourantas

Department of Cardiology, Barts Heart Centre, Barts Health NHS, London, United Kingdom

Email: cbourantas@gmail.com

Dr Bourantas and Dr Zanchin contributed equally to the preparation of this manuscript.

ABSTRACT

Objectives

This study examined the value of endothelial shear stress (ESS) estimated in 3-dimensional quantitative coronary angiography (3D-QCA) models in detecting plaques that are likely to progress and cause events.

Background

Cumulative evidence has shown that plaque characteristics and ESS derived from intravascular ultrasound (IVUS)−based reconstructions enable prediction of lesions that will cause cardiovascular events. However, the prognostic value of ESS estimated by 3D-QCA in nonflow limiting lesions is yet unclear.

Methods

This study analyzed baseline virtual histology (VH)-IVUS and angiographic data from 28 lipid-rich lesions (i.e., fibroatheromas) that caused major adverse cardiovascular events or required revascularization (MACE-R) at 5-year follow-up and 119 lipid-rich plaques from a control group that remained quiescent. The segments studied by VH-IVUS at baseline were reconstructed using 3D-QCA software. In the obtained geometries, blood flow simulation was performed, and the pressure gradient across the lipid-rich plaque and the mean ESS values in 3-mm segments were estimated. The additive value of these hemodynamic indexes in predicting MACE-R beyond plaque characteristics was examined.

Results

MACE-R lesions were longer, had smaller minimum lumen area, increased plaque burden (PB), were exposed to higher ESS, and exhibited a higher pressure gradient. In multivariable analysis, PB (hazard ratio: 1.08; p = 0.004) and the maximum 3-mm ESS value (hazard ratio: 1.11; p = 0.001) were independent predictors of MACE-R. Lesions exposed to high ESS (>4.95 Pa) with a high-risk anatomy (minimal lumen area <4 mm^2 and PB >70%) had a higher MACE-R rate (53.8%) than those with a low-risk anatomy exposed to high ESS (31.6%) or those exposed to low ESS who had high- (20.0%) or low-risk anatomy (7.1%; p < 0.001).

Conclusions

In the present study, 3D-QCA-derived local hemodynamic variables provided useful prognostic information, and, in combination with lesion anatomy, enabled more accurate identification of MACE-R lesions.

Key Words

quantitative coronary angiography, shear stress, vulnerable plaque

Central illustration

Major adverse cardiovascular event – revascularization rate of lesions with and without virtual histology-intravascular ultrasound-defined high-risk plaque characteristics exposed to high or low maximum ESS.

Thin-capped fibroatheroma (TCFA) (+) indicates the lesions with a TCFA phenotype, minimum lumen area (MLA) (+) the lesions with MLA ≤4.0 mm2, plaque burden (PB) (+) the lesions with PB ≥70%, and endothelial shear stress (ESS) (+) the lesions exposed to high maximum ESS (>4.95 Pa).

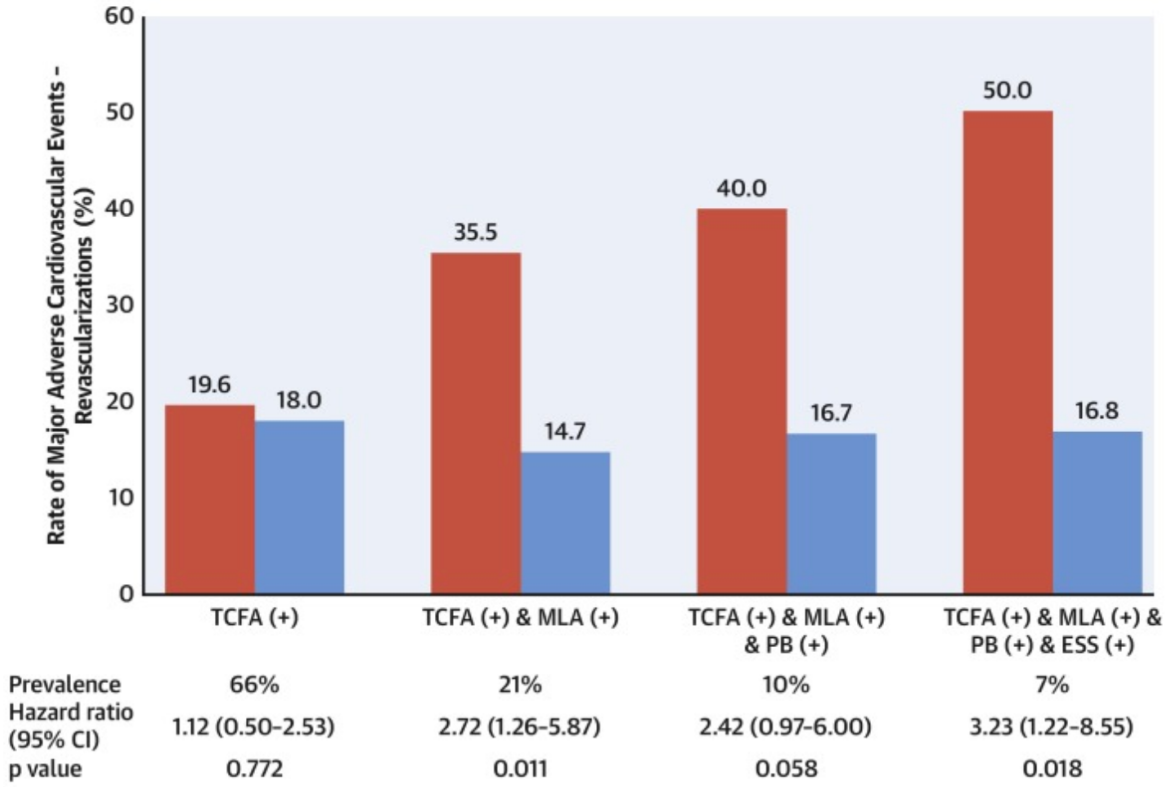

Abbreviations and Acronyms

3D:	3-dimensional
DS:	diameter stenosis
ESS:	endothelial shear stress
IQR:	interquartile range
MACE-R:	major adverse cardiovascular events–revascularization
MLA:	minimum lumen area
MLD:	minimum lumen diameter
QCA:	quantitative coronary angiography
PB:	plaque burden
TCFA:	thin cap fibroatheroma
ThCFA:	thick cap fibroatheroma
VH-IVUS:	virtual histology intravascular ultrasound

INTRODUCTION

Prospective invasive imaging studies of coronary atherosclerosis have provided robust evidence that intravascular imaging can identify, but only with modest accuracy, vulnerable plaques that are likely to progress and cause cardiovascular events (1,2). Computational fluid dynamic analysis of models reconstructed by intravascular imaging data and estimation of the local hemodynamic forces appear to provide additional prognostic information. Recent reports have shown that when they are combined with plaque characteristics, they enable accurate detection of lesions that can progress and cause events (3,4). However, intravascular imaging−based reconstruction and blood flow simulation processing is a tedious and time-consuming process that requires dedicated software and expertise, thus limiting its use in everyday clinical practice.

Conversely, 3-dimensional quantitative coronary angiography (3D-QCA) can be performed in real-time while the patient is in the catheterization laboratory. This technique appears to accurately assess lumen dimensions, as well as the extent and the severity of coronary artery disease. Recently, we processed 3D-QCA models with computational fluid dynamic techniques and demonstrated that the estimated endothelial shear stress (ESS) was a predictor of atherosclerotic disease progression at 1-year follow-up (5). In addition, a post hoc analysis of the FAME (Fractional Flow Reserve versus Angiography for Multivessel Evaluation) II study showed that the 3D-QCA-derived ESS estimated in hemodynamically severe stenoses predicted stenoses that caused myocardial infarction at 3-year follow-up (6). However, the combined value of plaque characteristics and of ESS estimated by 3D-QCA in nonflow limiting plaques in predicting stenoses that are likely to progress and cause events is yet unclear.

METHODS

Studied patients

The present study is a post hoc analysis of data acquired from the PROSPECT (Providing Regional Observations to Study Predictors of Events in the Coronary Tree) and IBIS-4 (Intergraded Biomarkers Imaging Study-4) studies. The design of both studies, the inclusion and exclusion criteria, and the endpoints and definitions were described in detail elsewhere (2,7). In brief, the PROSPECT trial was a large-scale prospective invasive imaging study that aimed to investigate the value of virtual histology-intravascular ultrasound (VH-IVUS) imaging in detecting vulnerable plaques that could progress and cause events. The study included 697 patients with acute coronary syndromes who had successful percutaneous coronary intervention in all culprit lesions and 3-vessel VH-IVUS imaging of the proximal 60- to 80-mm segment. The IBIS 4 study was a multicenter multimodality imaging study that aimed to examine the effect of aggressive statin therapy (rosuvastatin 40 mg once daily) on plaque burden (PB) and composition in patients admitted with ST-segment elevation myocardial infarction. All the recruited patients (n = 103) had successful revascularization and underwent 3-vessel VH-IVUS and optical coherence tomography imaging of the proximal 50-mm segment at baseline and at 13-month follow-up. The patients recruited in the PROSPECT study were followed for a median of 3.4 years, whereas those recruited in the IBIS-4 study were followed for 5 years. Both studies complied with the Declaration of Helsinki and were approved by the ethics committees of all the participant centers.

Clinical endpoints

The primary endpoint of the PROSPECT study was the composite endpoint of cardiac death or arrest, myocardial infarction, or rehospitalization for unstable or progressive angina. The

IBIS-4 study had an imaging-based endpoint (i.e., the change in the percent atheroma volume at 13-month follow-up). However, in the IBIS 4 study, which was a sub-study of the COMFORTable-AMI (Comparison of Biolimus Eluted from an Erodible Stent Coating with Bare Metal Stents in Acute ST-Elevation Myocardial Infarction) study, clinical endpoints were also recorded, including cardiac death, myocardial infarction, and target and nontarget lesion revascularization. In the IBIS 4 study, revascularization was deemed clinically indicated at follow-up angiography when there was a percent diameter stenosis (%DS) of ≥70% on QCA or 70% ≥ %DS ≥50% and recurrent angina or evidence of ischemia at rest or during an exercise test.

The clinical, angiographic, and intravascular imaging data in both studies enabled identification of untreated lesions that were assessed by VH-IVUS at baseline and caused events. The present analysis focused on these lesions; the primary endpoint of this study was the combined endpoint of cardiac death, myocardial infarction, or revascularization because of progressive or unstable angina, because of evidence of ischemia and 70% ≥ %DS ≥ 50% on follow-up coronary angiography, or because of significant disease progression (%DS ≥70%) at follow-up angiography (MACE-R). The secondary endpoint of the present analysis was the combined endpoint of cardiac death, myocardial infarction, or revascularization because of progressive or unstable angina (MACE).

Studied lesions and VH-IVUS analysis

In the PROSPECT study, 25 of the untreated lesions at baseline that were studied by VH-IVUS and caused events had a thin cap fibroatheroma (TCFA) phenotype, 18 untreated lesions had a thick cap fibroatheroma (ThCFA) phenotype, 7 had a non-fibroatheroma phenotype, and 4 were unclassified lesions. In the IBIS 4 study, all the lesions associated

with MACE-R had either a TCFA (n = 13) or a ThCFA (n = 2) phenotype (2,4). The present analysis included only untreated lesions with a lipid-rich phenotype (TCFA or ThCFA) that caused MACE-R during follow-up and a 4-fold sample of lesions with a lipid-rich phenotype that remained quiescent. Lesions that were short (<9 mm), those with suboptimal angiographic images (i.e., poor opacification of lumen silhouette, excessive foreshortening, or overlapping), and cases in which the DICOM (Digital Imaging and Communications in Medicine) file did not include all the necessary information for 3D-QCA reconstruction were excluded from the analysis.

VH-IVUS data analysis was performed by independent core laboratories (Cardiovascular Research Foundation, New York, New York in PROSPECT and Cardialysis B.V., Rotterdam, the Netherlands in IBIS-4). Classification of remodeling pattern and lesion phenotype was performed in both core laboratories using the same protocol (Supplemental Appendix). For each lesion with a TCFA or ThCFA phenotype its remodeling pattern, its length, the length of the proximal shoulder of the lesion, the distance ostium of the studied vessel to minimum lumen area (MLA) of the lesion, its MLA, external elastic membrane, plaque area, and PB at the MLA were estimated and recorded.

3D-QCA reconstruction, blood flow simulation, and data processing

Anatomical landmarks (i.e., side branches) seen in both IVUS and x-ray angiography were used to identify the proximal and distal end of the "segment of interest" (i.e., the segment that was assessed by VH-IVUS) on coronary angiography. Two end-diastolic angiographic projections (>25° apart) where there was no overlapping or foreshortening of the segment of interest and that allowed accurate delineation of the lumen silhouette were selected and used to reconstruct its anatomy using well-validated software (QAngio XA 3D RE, Medis, Leiden,

the Netherlands) (8). The distances proximal end of the segment of interest to the proximal end of each TCFA/ThCFA and distal end of the segment of interest to the distal end of each TCFA/ThCFA were used to identify lesion location in 3D-QCA models. Then, 3D-QCA analysis was performed for each lesion, and the lesion length, minimum lumen diameter (MLD), and %DS were estimated.

The 3D-QCA models were processed with computational fluid dynamic techniques, and the ESS distribution was estimated (Supplemental Appendix). The location of each TCFA/ThCFA lesion was identified in the 3D-QCA models and the lesion was then divided into consecutive 3-mm segments. The ESS values were extracted across the circumference and length of the segment for each of these segments, and the mean value was calculated (3,4). For each lesion, the highest and lowest mean ESS values, estimated in the 3-mm segments of the lesion, were recorded and defined the maximum and minimum lesion ESS, respectively.

Statistical analysis

Numerical variables are presented as median (interquartile range [IQR]), whereas categorical variables are presented as absolute values and percentages. The Mann-Whitney U test was used to compare numerical variables between lesions associated with MACE-R or MACE and those that remained quiescent, whereas categorical variables were compared using the chi-square test. Cox regression analysis was used to identify VH-IVUS, 3D-QCA, and 3D-QCA-derived hemodynamic predictors associated with MACE-R or MACE. Receiver-operating characteristics curve analysis was performed for each variable associated with MACE-R ($p < 0.05$); those with the highest area under the curve that were not collinear ($r < 0.50$) were entered into a multivariate model.

Receiver-operating characteristics curve analysis was also used for the computational fluid dynamic-derived variables to identify the best cutoff that predicted MACE-R; this was used to classify lesions in groups. Kaplan-Meier plots were used to display time to event at lesion and patient levels; comparison of the MACE-R rate between groups with different plaque characteristics and hemodynamic profiles was performed using the log-rank test. Lesions or patients with no events were censored at the latest contact date. In case of multiple lesions in the same patient, the lesion with the highest maximum ESS value or the lesion that exhibited the highest pressure gradient was used in the patient-level analysis. Analyses were performed in Stata version 15.1 (StataCorp LP, College Station, Texas) and R version 3.4.2 (R Foundation, Vienna, Austria). A p value <0.05 was considered statistically significant.

RESULTS

Patient demographics

In the PROSPECT study, 54 MACE occurred during a median of 3.4 years of follow-up. In the IBIS 4 study, 15 MACE-R events occurred (9 cardiac events and 6 revascularizations) within 5 years of follow-up. After excluding cases who had IVUS analysis or co-registration with coronary angiography was not possible, cases in whom there was insufficient information for 3D-QCA reconstruction in the DICOM files, lesions with short length, and those with a nonlipid-rich phenotype, 28 MACE-R lesions (n = 26) were included in the present analysis (16 from the PROSPECT study and 12 from the IBIS-4 study). Revascularization was performed in 6 lesions during invasive assessment at 13-month follow-up either because of new-onset angina and a $70\% \geq \%DS \geq 50\%$ (n = 1) or significant disease progression (DS >70%; n = 5) in follow-up coronary angiography (Figure 1).

The control group consisted of the non-MACE lipid-rich lesions included in the PROSPECT ESS sub-study that investigated the efficacy of ESS estimated in IVUS-based models in predicting events (n = 122) (4), and the non−MACE-R lesions with a lipid-rich phenotype (n = 74) identified in patients recruited in the IBIS-4 study at Bern University Hospital. From these lesions, 16 cases were excluded because of suboptimal angiographic image quality, and 61 were excluded because of lack of sufficient information in the DICOM file for 3D-QCA analysis. Therefore, the final control group consisted of 119 non-MACE-R lipid-rich lesions (53 from the PROSPECT and 66 from the IBIS-4 study) (Figure 1).

A total of 92 patients (45 recruited from PROSPECT and 47 from the IBIS 4 study; 119 vessels) were included in the present analysis. As shown in Table 1, there were no significant differences in the baseline demographics between the patients who experienced MACE-R and the control group. The baseline demographics of the patients recruited in the PROSPECT and IBS 4 studies are shown in Supplemental Table 1.

Characteristics and ESS distribution of lesions

Coronary reconstruction and blood flow simulation was successfully performed in all the studied vessels (n = 147). The median length of reconstructed segments was 44.1 mm (IQR: 34.3 to 56.2 mm), which yielded 1,882 3-mm segments; the median mean ESS was 2.19 Pa (IQR: 1.46 to 3.39 Pa). The IVUS MLA coincided with the 3D-QCA MLA in 40% of studied lesions; in the remaining lesions, IVUS MLA was located in a different 3-mm segment than the 3D-QCA MLA. The distribution of the ESS across the studied lesions is shown in the Supplemental Figure 1.

Table 2 shows the morphological, angiographic, and hemodynamic characteristics of the studied lesions. MACE-R lesions were longer on VH-IVUS, had a smaller MLA, and increased PB compared with non-MACE-R lesions. Conversely, the 3D-QCA lesion length was not different between groups; however, the lesions associated with MACE-R had a higher %DS and a smaller MLD. The maximum ESS values and the pressure drop across the MACE-R lesions were higher compared with non-MACE-R lesions. There were no differences between groups in the incidence of TCFA, minimum ESS values, and location of MACE-R and non-MACE-R lesions in the coronary tree. Similar findings were noted for the morphological, angiographic, and hemodynamic characteristics of the lesions that caused MACE (n = 22) (Supplemental Table 2).

Predictors of MACE-R and MACE: lesion-level analysis

Three VH-IVUS-derived variables (lesion length, MLA, and PB), 2 3D-QCA-derived variables (MLD and %DS), and 2 hemodynamic variables (maximum ESS value, pressure drop across the lesion) were predictors of MACE-R lesions (Table 3). By multivariable analysis, PB and maximum ESS were independent predictors of MACE-R lesions. Maximum ESS was the only independent predictor of MACE-R when the MLA was entered into the multivariate model (hazard ratio: 1.08; 95% confidence interval: 1.02 to 1.16; p = 0.016). Similar results were reported when analysis was performed only for lesions with a TCFA phenotype (Supplemental Table 3).

The best maximum ESS cutoff for predicting MACE-R lesions was 4.95 Pa, whereas the best cutoff for the pressure drop was 2.31 mm Hg. Lesions were classified into 4 groups according to the presence of ≥2 of the 3 high-risk plaque characteristics that in the PROSPECT study were associated with MACE (MLA ≤4 mm2, PB ≥70%, TCFA phenotype) and the maximum

ESS value (>4.95 Pa or <4.95 Pa) (9). As shown in Figure 2A, lesions with a high-risk plaque morphology exposed to high ESS had worse prognosis than lesions exposed to high ESS with a low-risk morphology or those exposed to low ESS. The results were not different when a high-risk plaque phenotype was defined as the presence of MLA ≤4 mm2 and PB ≥70% or when the pressure gradient across the lesion (>2.31 mmHg) was used to define an unfavorable hemodynamic environment (Figures 2B to 2D). The additive value of the maximum lesion ESS over the established VH-IVUS−derived, high-risk plaque characteristics in predicting MACE-R is shown in Figure 3 and the Central Illustration.

Lesions were classified in groups according to the presence or absence of (A) ≥2 high-risk plaque features and increased maximum endothelial shear stress (ESS) values (>4.95 Pa), (B) ≥2 high-risk plaque features and a high-pressure gradient (>2.31 mm Hg) across the lesion, (C) plaque burden (PB) ≥70%, minimum lumen area (MLA) ≤4 mm2, and increased maximum ESS, and (D) PB ≥70%, MLA ≤4 mm2, and a high-pressure gradient. Abbreviations as in Figure 1.

Similar results were reported when analysis was performed for the MACE lesions. VH-IVUS−derived MLA and PB, 3D-QCA-derived MLD, %DS, maximum ESS, and the pressure gradient were predictors of MACE. In multivariate analysis, PB and maximum ESS were the only independent predictors of MACE (Table 4). Maximum ESS was the only independent predictor of MACE when the MLA was entered into the multivariate model (hazard ratio: 1.09; 95% confidence interval: 1.02 to 1.17; p = 0.011). Kaplan-Meier analysis of the MACE rate according to lesion morphological characteristics and maximum ESS or pressure gradient across the lesion is shown in Figure 4.

Predictors of MACE-R: patient-level analysis

At a patient level, MLA, PB, MLD, %DS, and the maximum ESS were predictors of MACE-R (Supplemental Table 4). Patients who had lipid-rich plaques with ≥2 high-risk plaque characteristics that were exposed to high ESS (>4.95 Pa) had worse prognosis than those with high-risk plaques exposed to low ESS (Figure 5). The pressure gradient across the lesion also appeared to provide additional prognostic information to plaque morphology; patients with lesions with ≥2 high-risk plaque characteristics that exhibited a pressure gradient >2.31 mm Hg had the worst prognosis compared with the other groups. Similar results were reported when high-risk lesions were defined as those with MLA ≤4 mm2 and a PB ≥70%.

DISCUSSION

For the first time, the present study evaluated the prognostic value of the 3D-QCA-derived hemodynamic indexes and plaque characteristics in stratifying nonflow limiting lesions that were likely to progress and cause MACE-R or MACE. We found that: 1) ESS distribution estimated in 3D-QCA models provided additional prognostic information and was an independent predictor of MACE-R or MACE; 2) the pressure gradient across nonflow limiting lipid-rich lesions was a predictor of MACE-R and/or MACE; 3) the combination of plaque characteristics and 3D-QCA-derived hemodynamic indexes (i.e., ESS or the pressure gradient across the lesion) enabled more accurate detection of MACE-R and MACE lesions than VH-IVUS-derived variables; and 4) plaque morphology and the hemodynamic variables estimated in 3D-QCA models allowed more accurate identification of the patients who were at risk to experiencing cardiovascular event than standalone VH-IVUS imaging.

Computational fluid dynamic-based animal and human studies have provided robust evidence about the role of the local hemodynamic forces on atherosclerotic disease progression and have highlighted their prognostic implications (9). Low ESS appears to promote, through mechano-transduction pathways, plaque evolution and the development of high-risk plaques and in clinical studies, low ESS was reported to be a predictor of lesions that progressed and caused events (3,10). Conversely, the role of high ESS on the formation of high-risk plaques is less well established; however, there is considerable evidence to suggest that high ESS contributes to the destabilization of vulnerable lesions (11,12). Despite the undoubted prognostic implications of ESS, blood flow simulation analyses have limited applications in the clinical arena. This should be at least partially attributed to the increased time required for coronary reconstruction and blood flow modeling.

In the present study we examined the prognostic value of 3D-QCA-derived hemodynamic variables in detecting nonflow-limiting lipid-rich plaques that are likely to progress and cause MACE-R. In contrast to findings reported in previous studies, we found that the maximum and not the minimum ESS predicted MACE-R and MACE (3,4). This discrepancy might be attributed to the different modality used to extract vessel geometry; 3D-QCA modeling has limited efficacy in assessing details in lumen morphology, which can affect ESS estimations, especially in complex long lesions that are likely to exhibit ESS heterogeneity (13). In the present study, in which the median lesion length was 22.7 mm, IVUS and 3D-QCA MLA co-located in only 40% of lesions, a finding that highlights the limited accuracy of 3D-QCA to accurately extract lumen architecture (Supplemental Figure 2). Taking into account the limitations of 3D-QCA and the fact that it generates smooth luminal surfaces, we used the mean rather the more commonly used minimum predominant ESS value to define the physiological profile of 3-mm segments (3,4).

Despite the limitations of 3D-QCA-modeling, the estimated hemodynamic indexes, and in particular, the ESS distribution provided useful prognostic information and improved the efficacy of established VH-IVUS-derived plaque characteristics in predicting events (Figure 3, Central Illustration). The maximum ESS was a predictor of lesion-related MACE-R/MACE in multivariable analysis, and the Kaplan-Meier plots demonstrated the synergetic effect of plaque morphology and ESS in predicting future MACE or angiographically indicated revascularizations. Two recent studies, the EMERALD (Exploring the Mechanism of Plaque Rupture in Acute Coronary Syndrome Using Coronary CT Angiography and Computational Fluid Dynamics) and a post hoc analysis from the FAME II reported similar findings to our analysis, demonstrating that the maximum ESS estimated in lesions reconstructed by computed tomography/coronary angiography or 3D-QCA were predictors of future myocardial infarctions (6,14). However, these studies included predominantly flow-limiting lesions (49% and 100% of the lesions included in the EMERALD and FAME II studies had fractional flow reserve ≤0.80, respectively) that should have been considered for revascularization. Conversely, our analysis focused on nonflow limiting stenoses, with a median pressure gradient across these lesions of only 1.95 mm Hg (IQR: 1.14 to 3.33 mm Hg), for which there was lack of evidence to support their invasive passivation. In addition, the EMERALD study predominantly included patients without a history of coronary artery disease who were less likely to have complex lesions, whereas in the FAME II study there was no information about plaque composition. Therefore, this analysis was unable to examine the additive predictive value of hemodynamic indexes over anatomic and morphological plaque characteristics derived by intravascular imaging. Finally, coronary reconstruction and blood flow simulation in both studies was computationally demanding because the EMERALD used computed tomographic coronary angiography derived models, whereas the FAME II study incorporated the side branches in the 3D-QCA models, which

considerably increased computation time. Conversely, our analysis included only the main branch and assumed steady coronary flow; this approach makes the real-time estimation of ESS feasible while the patient is in the catheterization laboratory.

The unfavorable implications of high ESS on plaque pathobiology is supported by several experimental studies that have shed light on the mechano-transduction pathways that regulate plaque evolution. High ESS promotes nitric oxide synthesis and proteolytic degradation of the fibrous cap by inhibiting extracellular matrix synthesis, as well as increases smooth muscle cell apoptosis and proteolytic matrix degradation (9). The preceding processes eventually result in fibrous cap fragility and rupture that can cause vessel thrombosis or plaque healing with accelerated disease progression (15). These events can have clinical manifestations if they occur in segments with increased PB and small MLA because in this setting they are likely to cause flow obstruction and ischemia (16). In our study, apart from ESS, increased PB and small MLA were also predictors of MACE-R, whereas PB was also an independent predictor of MACE-R in the multivariate Cox regression analysis.

Interestingly, apart from ESS, the pressure gradient across the lesion estimated in our 3D-QCA models also provided useful prognostic information and was a predictor of MACE-R and MACE. Kaplan-Meier analysis showed that lesions with a high pressure gradient (and especially those with high-risk plaque characteristic) had a poor prognosis, with event rates as high as 51.8% at 5-year follow-up. Several studies demonstrated that a low fractional flow reserve was a predictor of worse outcomes even in angiographically nonflow limiting stenoses (17). In these studies, the prognostic value of fractional flow reserve was attributed to the fact that it reflected atherosclerotic burden. However, in our analysis and in the EMERALD study, the pressure gradient seemed to provide additional prognostic information

beyond plaque characteristics. An increased pressure gradient across a lesion is associated with increased axial tensile stress, flow disturbances and ESS heterogeneity; this unfavorable hemodynamic environment can accelerate atherosclerotic evolution, leading to plaque destabilization and future events (18,19).

The findings of the present analysis provide evidence of the value of 3D-QCA−derived hemodynamic indexes in identifying vulnerable plaques (Supplemental Figure 3). Software have been developed that enable real-time computation of the fractional flow reserve from 3D-QCA, which could be used in future studies to enhance the efficacy of intravascular imaging in detecting plaques prone to progress and cause events (20).

Moreover, the present analysis also underscore the potential value of plaque morphology and physiology (i.e., ESS distribution or pressure drop across a lesion) in stratifying cardiovascular risk. The models that are currently available to identify high-risk patients rely either on patient demographics or on the combination of clinical and imaging biomarkers and they have modest predictive accuracy (21). The patient-level analysis of our study showed that the subjects with high-risk plaques and an unfavorable local hemodynamic environment had a high event rate during follow-up. Further research is needed to examine the potential value of noninvasive or invasive assessment of plaque pathology (i.e., plaque burden and composition) and physiology in identifying patients at risk who would benefit from emerging therapies that target atherosclerosis.

Study limitations

A significant limitation of the present analysis was that only 48% of the lipid-rich lesions that caused MACE-R were suitable for inclusion. This might have introduced selection bias and resulted in a small sample size and events that did not allow us to accurately quantify the additive value of hemodynamic variables over VH-IVUS−derived plaque characteristics in predicting MACE-R. Therefore, the reported results should be interpreted with caution and require further confirmation in future large-scale studies.

In addition, in some of the angiograms from the PROSPECT study, the pixel size was not available; thus, vessel reconstruction relied on a manual calibration that could affect the accuracy of 3D-QCA modeling. Moreover, we performed steady flow simulation, which assumed that blood was a Newtonian fluid, and we did not include side branches in the 3D-QCA models. Steady flow simulation can accurately predict time-averaged ESS in pulsatile simulations (22). Conversely, a Newtonian assumption might not accurately approximate blood behavior, especially in diseased segments where more regions of slow flow are expected (23). In addition, the incorporation of the side branches in the 3D models was expected to enable more accurate assessment of the ESS distribution; however, a recent study showed that incorporation of the side branches into the 3D vessel geometry only marginally improved the accuracy of the ESS in predicting plaque evolution (24). Complex simulation, especially in complex geometries, is time consuming and cannot be performed in the catheterization laboratory. With the proposed approach, ESS, and especially, the pressure drop across a lesion, can be computed fast in single-vessel geometries. Currently, QCA reconstruction and blood flow simulation takes approximately 15 min; however, developments in software design and advances in computer technology are expected to

reduce this time to a few minutes, enabling the real-time computation of 3D-QCA-derived ESS.

Furthermore, VH-IVUS imaging was performed using 2 different imaging systems (Invision Gold in PROSPECT and s5 in IBIS 4 [Volcano Corp., Rancho Cordova, California]; VH analysis from these 2 systems might provide different estimations for plaque composition and phenotype. In addition, follow-up coronary angiography and revascularization because of disease progression on angiography was performed only in the IBIS 4 study, whereas the follow-up period (median 3.4 years in the PROSPECT and 5 years in the IBIS-4) was different in the 2 studies. However, it is reassuring that our findings were similar when analysis was restricted to MACE or to the first 3.4 years of follow-up (Supplemental Figure 4).

Finally, the number of the events reported in this analysis was relatively small, and most of the events were unstable or progressive angina and not hard clinical endpoints (death, myocardial infarction). However, we must acknowledge that in all the prospective multivessel intravascular imaging studies of coronary atherosclerosis, the incidence of hard endpoints is low (1, 2, 3). In addition, the clinical endpoints of this study were similar to the endpoints of the recently completed Lipid Rich Plaque study and of ongoing studies of coronary atherosclerosis (PROSPECT II [PROSPECT II & PROSPECT ABSORB–An Integrated Natural History Study and Randomized Trial. (P2)]; NCT02171065; PREVENT [The Preventive Coronary Intervention on Stenosis With Functionally Insignificant Vulnerable Plaque]; NCT02316886; COMBINE [Optical Coherence Tomography Morphologic and Fractional Flow Reserve Assessment in Diabetes Mellitus Patients];

NCT02989740) that are expected to provide additional data and the substrate to prove the concept introduced in this study.

CONCLUSIONS

In the present analysis of the PROSPECT and IBIS 4 studies, hemodynamic indexes estimated from 3D-QCA models provided additional prognostic information to VH-IVUS−derived variables and enabled more accurate detection of nonflow limiting lesions that were likely to progress and cause events. Prospective studies are needed to confirm these findings and examine the efficacy of intravascular imaging and 3D-QCA-derived variables in detecting high-risk lesions and patients who may benefit from preemptive focal or systemic treatment of atherosclerosis.

PERSPECTIVES

Competency in medical knowledge: In this post hoc analysis of the PROSPECT and IBIS 4 imaging studies, ESS estimated in 3D-QCA-derived models improved the predictive efficacy of VH-IVUS in identifying lesions prone to exhibit disease progression and cause MACE-R at 5-year follow-up.

Translational outlook: Future developments in software design are expected to enable fast computation of ESS distribution in 3D-QCA models and facilitate the conduction of large-scale studies that will assess the potential value of 3D-QCA-derived ESS in predicting lesions that are likely to progress and cause cardiovascular events.

REFERENCES

1. R. Walksam, C. Di Mario, R. Torguson, Identification of patients and plaques vulnerable to future coronary events with near-infrared spectroscopy intravascular ultrasound imaging: a prospective, cohort study, Lancet, 394 (2019), pp. 1629-1637.
2. G.W. Stone, A. Maehara, A.J. Lansky, et al. A prospective natural-history study of coronary atherosclerosis N Engl J Med, 364 (2011), pp. 226-235.
3. P.H. Stone, S. Saito, S. Takahashi, et al. Prediction of progression of coronary artery disease and clinical outcomes using vascular profiling of endothelial shear stress and arterial plaque characteristics: the PREDICTION Study, Circulation, 126 (2012), pp. 172-181.
4. P.H. Stone, A. Maehara, A.U. Coskun, et al. Role of low endothelial shear stress and plaque characteristics in the prediction of nonculprit major adverse cardiac events: the PROSPECT study, J Am Coll Cardiol Img, 11 (2018), pp. 462-471.
5. C.V. Bourantas, A. Ramasamy, A. Karagiannis, et al. Angiographic derived endothelial shear stress: a new predictor of atherosclerotic disease progression, Eur Heart J Cardiovasc Imaging, 20 (2019), pp. 314-322.
6. A. Kumar, E.W. Thompson, A. Lefieux, et al. High coronary shear stress in patients with coronary artery disease predicts myocardial infarction, J Am Coll Cardiol, 72 (2018), pp. 1926-1935.
7. L. Raber, M. Taniwaki, S. Zaugg, et al. Effect of high-intensity statin therapy on atherosclerosis in non-infarct-related coronary arteries (IBIS-4): a serial intravascular ultrasonography study, Eur Heart J, 36 (2015), pp. 490-500.
8. S. Tu, Z. Huang, G. Koning, K. Cui, J.H. Reiber, A novel three-dimensional quantitative coronary angiography system: in-vivo comparison with intravascular ultrasound for assessing arterial segment length, Catheter Cardiovasc Interv, 76 (2010), pp. 291-298.

9. V. Thondapu, C.V. Bourantas, N. Foin, I.K. Jang, P.W. Serruys, P. Barlis. Biomechanical stress in coronary atherosclerosis: emerging insights from computational modelling, Eur Heart J, 38 (2017), pp. 81-92.
10. Y.S. Chatzizisis, A.B. Baker, G.K. Sukhova, et al. Augmented expression and activity of extracellular matrix-degrading enzymes in regions of low endothelial shear stress colocalize with coronary atheromata with thin fibrous caps in pigs, Circulation, 123 (2011), pp. 621-630.
11. R. Torii, R. Stettler, L. Raber, et al. Implications of the local hemodynamic forces on the formation and destabilization of neoatherosclerotic lesions, Int J Cardiol, 272 (2018), pp. 7-12.
12. Y. Fukumoto, T. Hiro, T. Fujii, et al. Localized elevation of shear stress is related to coronary plaque rupture: a 3-dimensional intravascular ultrasound study with in-vivo color mapping of shear stress distribution, J Am Coll Cardiol, 51 (2008), pp. 645-650.
13. A.P. Antoniadis, M.I. Papafaklis, S. Takahashi, et al. Arterial remodeling and endothelial shear stress exhibit significant longitudinal heterogeneity along the length of coronary plaques, J Am Coll Cardiol Img, 9 (2016), pp. 1007-1009.
14. J.M. Lee, G. Choi, B.K. Koo, et al. Identification of High-Risk Plaques Destined to Cause Acute Coronary Syndrome Using Coronary Computed Tomographic Angiography and Computational Fluid Dynamics, J Am Coll Cardiol Img, 12 (2019), pp. 1032-1043.
15. M.J. Davies, A.C. Thomas. Plaque fissuring--the cause of acute myocardial infarction, sudden ischaemic death, and crescendo angina, Br Heart J, 53 (1985), pp. 363-373.
16. J. Tian, X. Ren, R. Vergallo, et al. Distinct morphological features of ruptured culprit plaque for acute coronary events compared to those with silent rupture and thin-cap fibroatheroma: a combined optical coherence tomography and intravascular ultrasound study, J Am Coll Cardiol, 63 (2014), pp. 2209-2216.

17. J.M. Lee, B.K. Koo, E.S. Shin, et al. Clinical implications of three-vessel fractional flow reserve measurement in patients with coronary artery disease, Eur Heart J, 39 (2018), pp. 945-951.
18. J.B. Park, G. Choi, E.J. Chun, et al. Computational fluid dynamic measures of wall shear stress are related to coronary lesion characteristics, Heart, 102 (2016), pp. 1655-1661.
19. C.J. Slager, J.J. Wentzel, F.J. Gijsen, et al. The role of shear stress in the destabilization of vulnerable plaques and related therapeutic implications, Nat Clin Pract Cardiovasc Med, 2 (2005), pp. 456-464.
20. C.V. Bourantas, H.M. Garcia-Garcia, R. Diletti, T. Muramatsu, P.W. Serruys. Early detection and invasive passivation of future culprit lesions: a future potential or an unrealistic pursuit of chimeras? Am Heart J, 165 (2013), pp. 869-881.e4.
21. C.V. Bourantas, H.M. Garcia-Garcia, R. Torii, et al. Vulnerable plaque detection: an unrealistic quest or a feasible objective with a clinical value? Heart, 102 (2016), pp. 581-589.
22. C.L. Feldman, O.J. Ilegbusi, Z. Hu, R. Nesto, S. Waxman, P.H. Stone. Determination of in vivo velocity and endothelial shear stress patterns with phasic flow in human coronary arteries: a methodology to predict progression of coronary atherosclerosis, Am Heart J, 143 (2002), pp. 931-939.
23. B. Liu, D. Tang. Influence of non-Newtonian properties of blood on the wall shear stress in human atherosclerotic right coronary arteries, Mol Cell Biomech, 8 (2011), pp. 73-90.
24. A. Sakellarios, C.V. Bourantas, S.L. Papadopoulou, et al. The effect of coronary bifurcation and haemodynamics in prediction of atherosclerotic plaque development: a serial computed tomographic coronary angiographic study, EuroIntervention, 13 (2017), Article e1084−91.

Table 1. Baseline Demographics of the Patients Who Experienced MACE-R and of the Control Group.

	Studied Patients (N = 92)	Patients Who Had MACE-R (n = 26)	Control Group (n = 66)	p Value
Age (yrs)	58.2 (51.5−64.8)	60.5 (53.5−67.0)	57.4 (50.9−64.3)	0.422
Male	81 (88)	24 (92)	57 (86)	0.429
BMI (kg/m^2)	27.1 (24.4−30.1)	27.5 (24.6−31.0)	27.0 (24.2−29.9)	0.643
Current smoker	47 (47)	14 (54)	27 (41)	0.261
Comorbidities				
Diabetes mellitus	15 (17)	7 (27)	9 (14)	0.130
Hypertension	42 (46)	11 (44)	31 (47)	0.800
Hypercholesterolemia	36 (40)	10 (44)	26 (39)	0.731
Renal failure*	3 (3)	1 (4)	2 (3)	0.764
Previous PCI	6 (7)	3 (11)	3 (4)	0.221
Family history of CAD	30 (33)	9 (39)	21 (33)	0.585
Clinical presentation				0.961
STEMI	58 (63)	16 (61)	42 (64)	
NSTEMI	30 (33)	9 (35)	21 (32)	
Unstable angina	4 (4)	1 (4)	3 (4)	
Medications at discharge				
Aspirin	91 (99)	26 (100)	65 (98)	0.528
Thienopyridines	92 (100)	100 (100)	45 (100)	–
Beta-blocker	87 (95)	23 (89)	64 (97)	0.105
RAAS inhibitor	76 (83)	20 (77)	56 (85)	0.367
Statin	88 (96)	25 (96)	63 (95)	0.882

Values are median (interquartile range) or n (%).

BMI = body mass index; CAD = coronary artery disease; MACE-R = major adverse cardiovascular event−revascularization; NSTEMI = non−ST-segment elevation myocardial infarction; PCI = percutaneous coronary intervention; RAAS = renin angiotensin aldosterone system; STEMI = ST-segment elevation myocardial infarction.

∗Renal failure was defined as an estimated glomerular filtration rate of <60 ml/min/1.73 m^2.

Table 2. Morphological and Hemodynamic Characteristics of the MACE-R Lesions and of Those That Remained Quiescent During Follow-Up

	Studied Lesions (N = 147)	MACE-R Lesions (n = 28)	Non-MACE-R Lesions (n = 119)	p Value
VH-IVUS plaque characteristics				
VH-IVUS lesion length (mm)	22.7 (12.9−35.2)	32.5 (18.0−41.6)	19.6 (12.7−31.3)	0.030
Distance vessel ostium to MLA (mm)	24.2 (10.2−35.9)	29.8 (15.1−44.6)	23.8 (9.2−34.3)	0.088
Length of the proximal shoulder (mm)	11.3 (6.6−23.1)	12.5 (6.5−18.2)	10.6 (6.6−23.3)	0.892
MLA (mm^2)	4.81 (3.68−6.30)	3.65 (3.26−4.36)	5.03 (3.98−6.66)	<0.001
EEM area (mm^2)	13.39 (10.53−16.11)	11.60 (10.64−14.66)	13.56 (10.41−16.53)	0.242
Plaque area (mm^2)	7.93 (6.56−10.62)	8.19 (7.08−10.55)	7.87 (6.21−10.72)	0.596
PB (%)	62.5 (55.0−68.8)	69.4 (63.5−72.0)	60.8 (53.7−66.5)	<0.001
TCFA phenotype	97 (66)	19 (67.9)	78 (65.5)	0.816
Remodeling pattern				0.309
Constrictive remodeling	81 (55.1)	17 (60.7)	64 (53.8)	
Compensatory remodeling	61 (41.5)	9 (32.1)	52 (43.7)	
Excessive expansive remodeling	5 (3.4)	2 (7.1)	3 (2.5)	
3D-QCA and CFD-derived variables				
3D-QCA lesion length (mm)	17.4 (13.0−25.2)	18.3 (14.3−25.1)	17.4 (12.4−25.4)	0.604
MLD (mm)	2.10 (1.78−2.52)	1.87 (1.52−2.05)	2.23 (1.84−2.56)	<0.001
Percentage DS (%)	25.9 (20.4−34.0)	36.5 (24.4−44.6)	24.9 (19.8−30.9)	0.001

	Studied Lesions (N = 147)	MACE-R Lesions (n = 28)	Non-MACE-R Lesions (n = 119)	p Value
Coronary blood flow (ml/s)	0.84 (0.63−1.17)	0.73 (0.56−1.12)	0.88 (0.66−1.17)	0.118
Maximum ESS value (Pa)	5.06 (3.23−8.91)	9.40 (6.30−12.52)	4.13 (2.99−6.96)	<0.001
Minimum ESS value (Pa)	1.21 (0.81−1.80)	1.17 (0.78−0.180)	1.33 (1.03−1.78)	0.296
Pressure drop across the lesion (mm Hg)	1.95 (1.14−3.33)	3.31 (2.28−5.17)	1.68 (0.97−2.67)	<0.001
Lesion location				
Coronary artery				0.212
Left anterior descending coronary artery	58 (39.5)	13 (46.4)	45 (37.8)	
Left circumflex coronary artery	44 (29.9)	11 (39.3)	33 (27.7)	
Right coronary artery	44 (99.9)	4 (14.3)	40 (33.6)	
Intermediate coronary artery	1 (0.7)	0 (0.0)	1 (0.8)	
Coronary segment				0.679
Proximal vessel	100 (68)	19 (68)	81 (68)	
Mid vessel	27 (18)	4 (14)	23 (19)	
Distal vessel	20 (14)	5 (18)	15 (13)	

Values are median (interquartile range) or n (%).

3D-QCA = 3-dimensional quantitative coronary angiography; CFD = computational fluid dynamics; DS = diameter stenosis; EEM = external elastic membrane; ESS = endothelial shear stress; MACE-R = major adverse cardiovascular events–revascularization; MLA = minimum lumen area; MLD = minimum lumen diameter; PB = plaque burden; TCFA = thin cap fibroatheroma; VH-IVUS = virtual histology intravascular ultrasound.

Table 3. Lesion-Level Univariable and Multivariable Analyses of the Morphological, Angiographic, and Hemodynamic Predictors of MACE-R.

	Univariable Analysis		Multivariable Analysis*	
	Hazard Ratio (95% CI)	**p Value**	**Hazard Ratio (95% CI)**	**p Value**
Lesion length (per 1-mm increase)	1.03 (1.00−1.05)	0.030	1.00 (0.98−1.03)	0.770
MLA (per 1-mm^2 increase)	0.53 (0.38−0.74)	<0.001	—	—
PB (per 1% increase)	1.10 (1.05−1.16)	<0.001	1.08 (1.03−1.14)	0.004
MLD (per 1-mm increase)	0.19 (0.08−0.44)	<0.001	—	—
Percentage DS (per 1% increase)	1.06 (1.03−1.10)	0.001	—	—
Maximum ESS value (per 1-Pa increase)	1.14 (1.08−1.20)	<0.001	1.11 (1.05−1.17)	0.001
Pressure drop across a lesion (per 1-mm Hg increase)	1.10 (1.03−1.18)	0.005	—	—

CI = confidence interval; other abbreviations as in Tables 1 and 2.

∗Significant correlation ($r > 0.50$) was noted between the maximum ESS and the MLA ($r = −0.612$; $p < 0.001$), the MLD ($r = −0.586$; $p < 0.001$); the %DS ($r = 0.518$; $p < 0.001$), and the pressure drop across the lesion ($r = −0.735$; $p < 0.001$). Maximum ESS was entered in the multivariate model because this variable had the highest area under the curve (AUC) in the receiver-operating characteristics analysis ($AUC_{maxESS} = 0.790$; $p < 0.001$; $AUC_{MLA} = 0.743$; $p < 0.001$; $AUC_{MLD} = 0.723$; $p < 0.001$; $AUC_{DS} = 0.711$; $p = 0.001$; $AUC_{pres\ drop} = 0.754$; $p < 0.001$).

Table 4. Lesion-Level Univariable and Multivariable Analyses of the Morphological, Angiographic, and Hemodynamic Predictors of MACE.

	Univariable Analysis		Multivariable Analysis*	
	Hazard Ratio (95% CI)	**p Value**	**Hazard Ratio (95% CI)**	**p Value**
MLA (per 1-mm^2 increase)	0.47 (0.31−0.72)	<0.001	—	—
PB (per 1% increase)	1.11 (1.05−1.17)	<0.001	1.09 (1.03, 1.16)	0.003
MLD (per 1-mm increase)	0.20 (0.08−0.51)	0.001	—	—
Percentage DS (per 1% increase)	1.05 (1.01−1.09)	0.008	—	—
Maximum 3-mm ESS value (per 1-Pa increase)	1.15 (1.09−1.22)	<0.001	1.12 (1.05, 1.19)	<0.001
Pressure drop across a lesion (per 1-mm Hg increase)	1.11 (1.03−1.19)	0.004	—	—

Abbreviations as in Tables 1, 2 and 3.

∗Significant correlation ($r > 0.50$) was noted between the maximum ESS and the MLA, the MLD, the %DS, and the pressure drop across the lesion. Maximum ESS was entered in the multivariate model as this variable had the highest AUC in the receiver-operating characteristics analysis ($AUC_{maxESS} = 0.797$; $p < 0.001$; $AUC_{MLA} = 0.787$; $p < 0.001$; $AUC_{MLD} = 0.737$; $p < 0.001$; $AUC_{DS} = 0.688$; $p = 0.005$; $AUC_{pres\ drop} = 0.779$; $p < 0.001$).

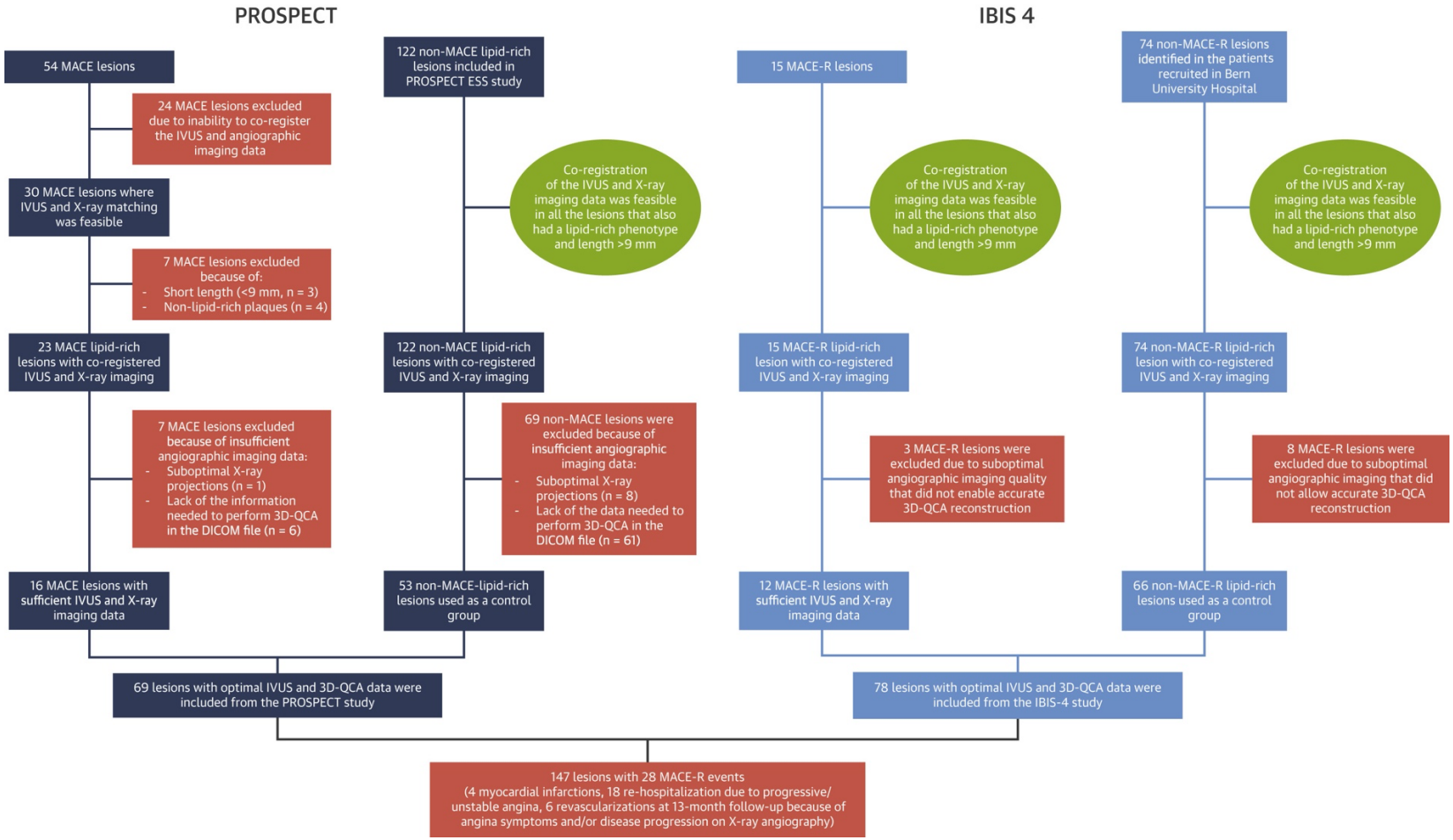

Figure 1. Study Design: Flowchart of the lesions included in the present analysis. 3D-QCA = 3-dimensional-quantitative coronary angiography; DICOM = Digital Imaging and Communications in Medicine; IVUS = intravascular ultrasound; MACE = major adverse cardiovascular event(s); MACE-R = major adverse cardiovascular event-revascularization.

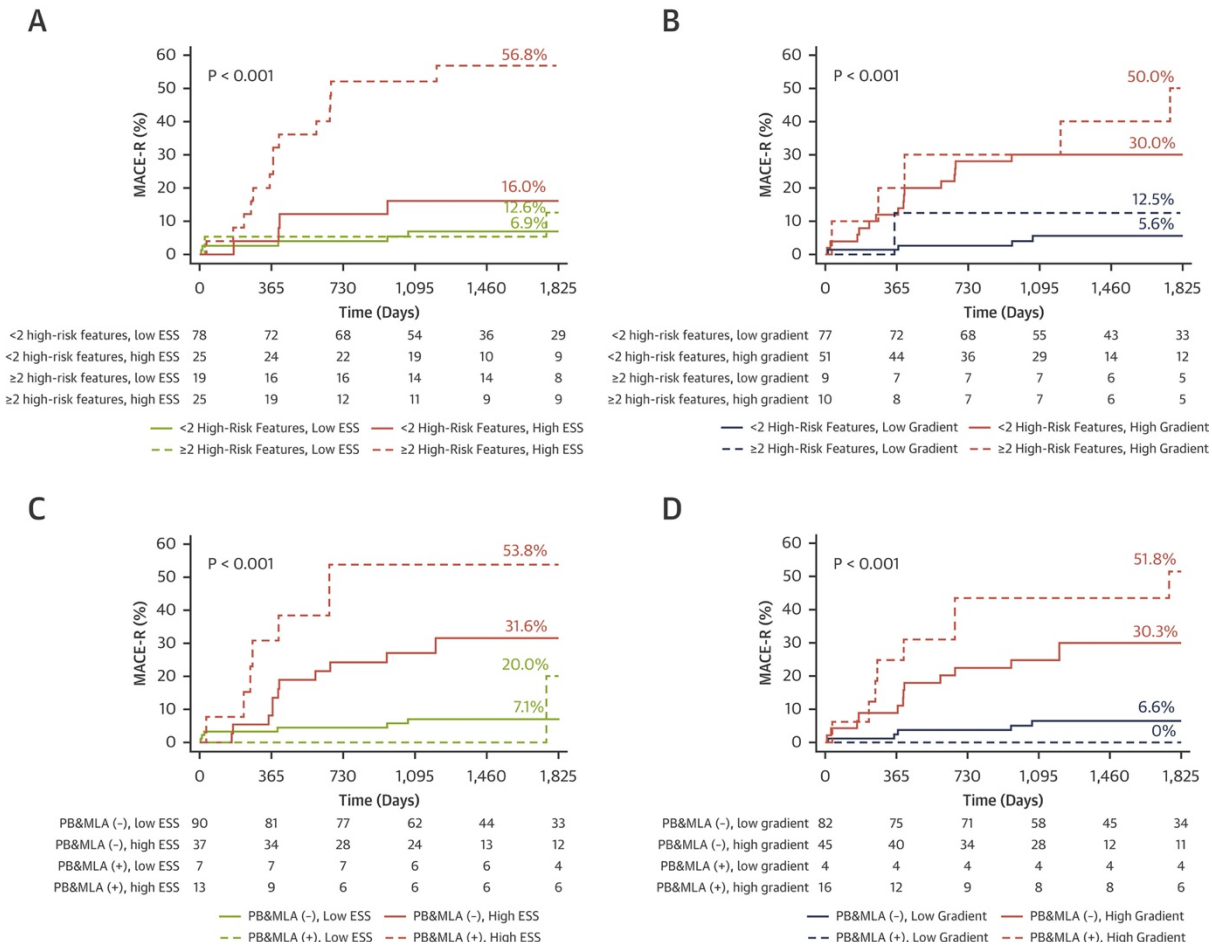

Figure 2. Kaplan-Meier Curves Showing MACE-R Rate According to Plaque and 3D-QCA-Derived Hemodynamic Indexes. Lesions were classified in groups according to the presence or absence of **(A)** ≥2 high-risk plaque features and increased maximum endothelial shear stress (ESS) values (>4.95 Pa), **(B)** ≥2 high-risk plaque features and a high-pressure gradient (>2.31 mm Hg) across the lesion, **(C)** plaque burden (PB) ≥70%, minimum lumen area (MLA) ≤4 mm^2, and increased maximum ESS, and **(D)** PB ≥70%, MLA ≤4 mm^2, and a high-pressure gradient. Abbreviations as in Figure 1.

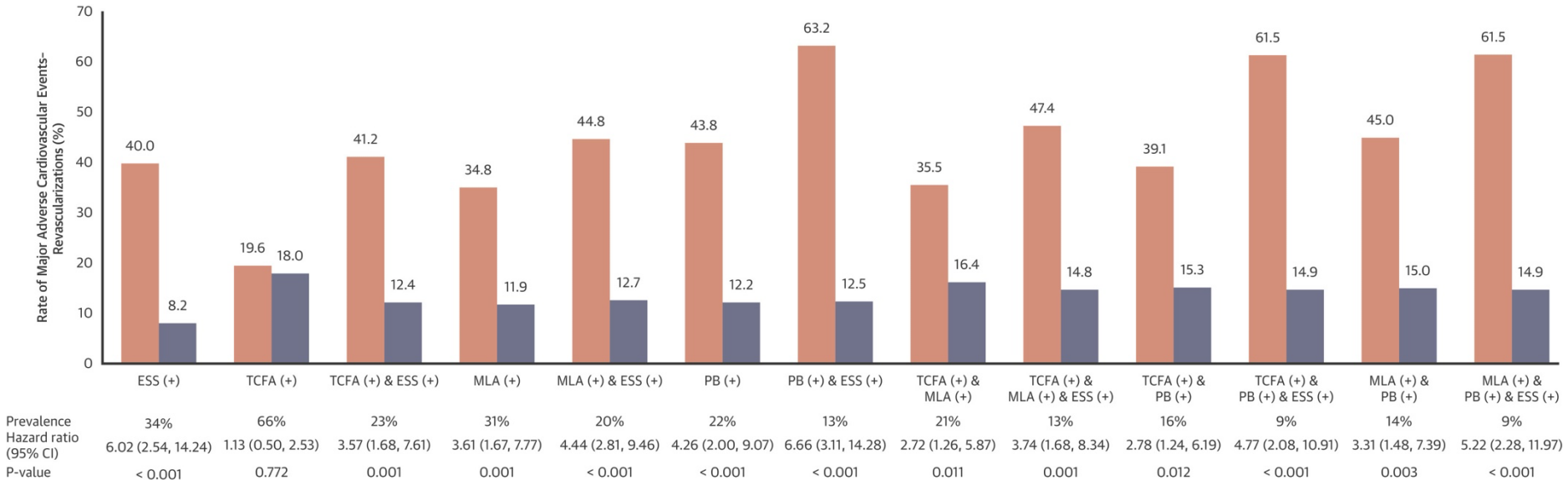

Figure 3. MACE-R Rate of Lesions With and Without VH-IVUS−Derived High-Risk Plaque Characteristics That Were or Were Not Exposed to High Maximum ESS Values. ESS (+) indicates lesions exposed to high maximum ESS (>4.95 Pa); thin-capped fibroatheroma (TCFA) (+) indicates the presence of a TCFA phenotype; MLA (+) a MLA ≤4.0 mm^2 and PB (+) a PB ≥70%. VH-IVUS = virtual histology-intravascular ultrasound; other abbreviations as in Figure 2.

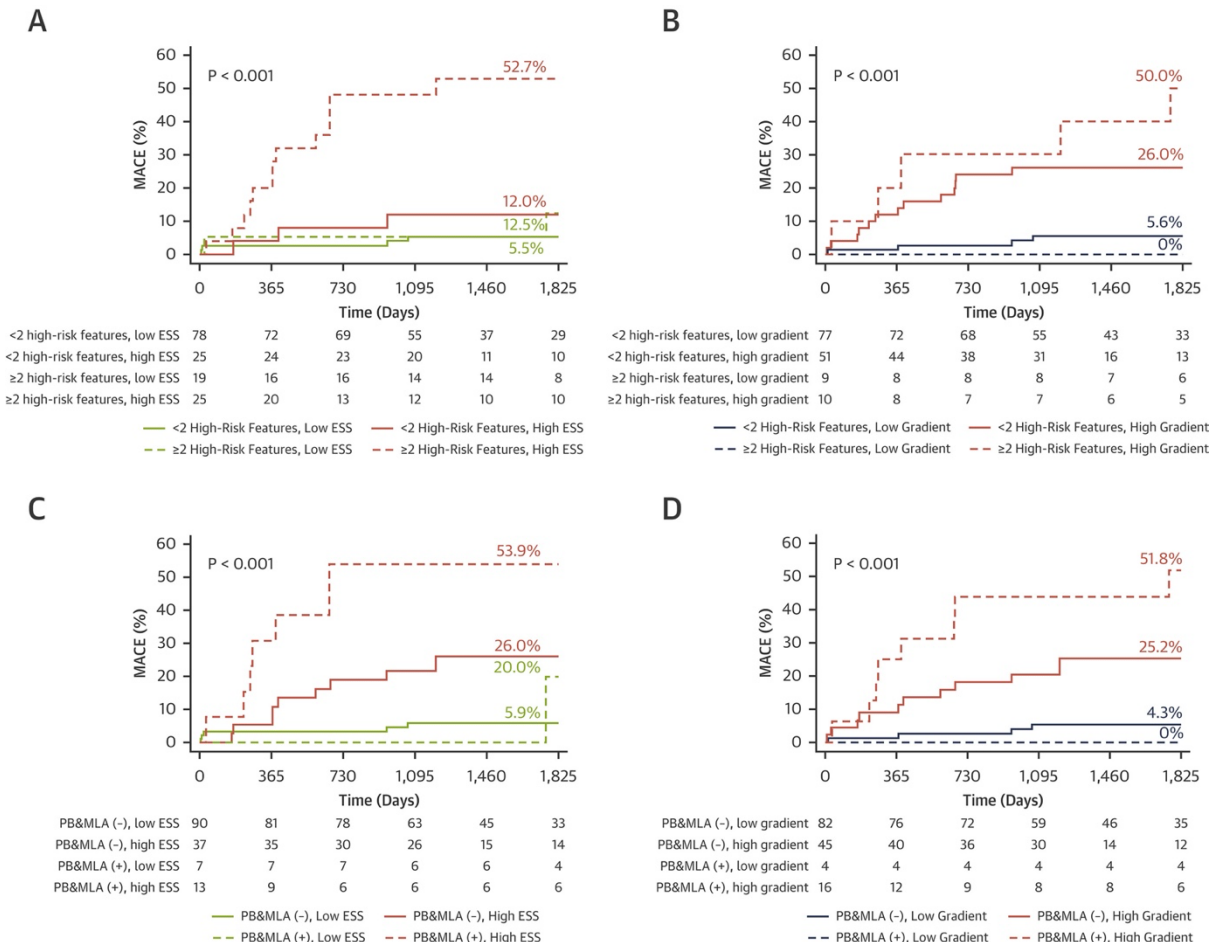

Figure 4. Kaplan-Meier Curves Showing MACE Rate According to Plaque And 3D-QCA−Derived Hemodynamic Indexes. Lesions were classified in groups according to the presence or absence of **(A)** ≥2 high-risk plaque features and increased maximum ESS values (>4.95 Pa), **(B)** ≥2 high-risk plaque features and a high-pressure gradient (>2.31 mm Hg) across the lesion, **(C)** PB ≥70% and MLA ≤4 mm^2 and increased maximum ESS values, and **(D)** PB ≥70% and MLA ≤4 mm^2 and a high-pressure gradient. Abbreviations as in Figures 1 and 2.

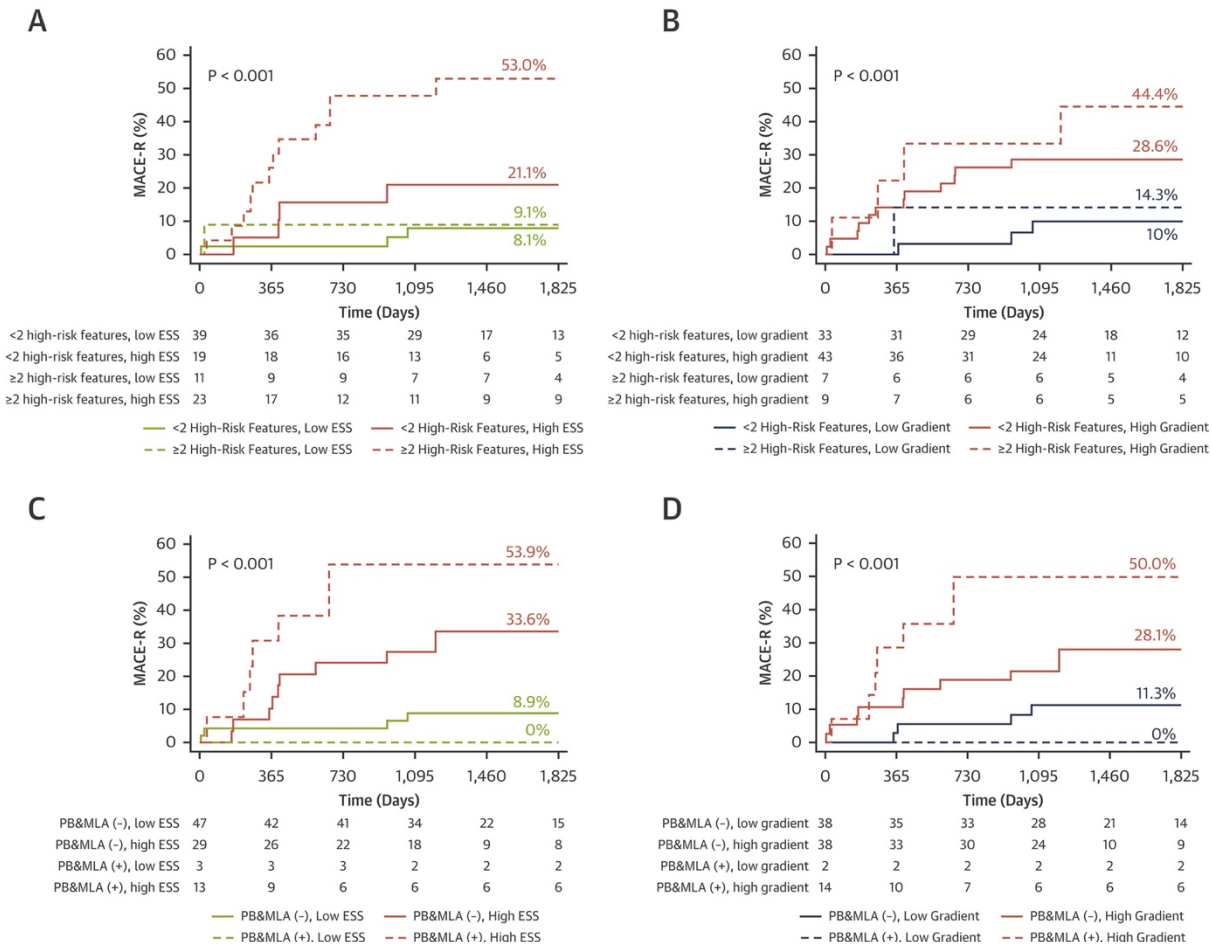

Figure 5. Kaplan-Meier Curves Showing Patient-Level MACE-R Rate According to Plaque And 3D-QCA−Derived Hemodynamic Indexes. Patients were classified in groups according to the presence or absence of **(A)** high-risk plaques (i.e., plaques with ≥2 high-risk features) and increased maximum ESS values (>4.95 Pa), **(B)** high-risk plaques and a high-pressure gradient (>2.31 mmHg) across the lesion, **(C)** PB ≥70% and MLA ≤4 mm^2 and increased maximum ESS values, and **(D)** lesions with PB ≥70%, MLA ≤4 mm^2, and a high-pressure gradient.